Ocean Systems Engineering, *Vol. 11, No. 2 (2021) 185-201*
DOI: https:// doi.org/10.12989/ose.2021.11.2.185

A comparison of smoothed particle hydrodynamics simulation with exact results from a nonlinear water wave model

Hoa X. Nguyen[1,3b], Van Nguyen Dinh[2a] and Biswajit Basu[*1]

[1]*School of Engineering, Trinity College Dublin, Ireland*
[2]*MaREI Centre for Energy, Climate and Marine, University College Cork, Ireland*
[3]*Faculty of Civil Engineering, Vietnam Maritime University, Hai Phong, Vietnam*

(Received August 28, 2019, Revised March 15, 2021, Accepted April 5, 2021)

Abstract. The aim of this paper is to verify the velocity profile and the pressure variation inside the fluid domain over one wavelength obtained from a numerically simulated Smoothed Particle Hydrodynamics model with some exact qualitative results (i.e., increasing/decreasing trend or constant value of a flow field) from a fully nonlinear Euler equation for water wave model. A numerical wave flume has been modeled and a regular wave train is created by the horizontal displacement of a wave paddle on one side of the flume. A passive beach is used to dissipate the energy of the wave on the other side. The extracted numerical results are compared with some recently available exact results from a nonlinear steady water wave model based on the Euler equations for irrotational flow. The flow properties under wave crests, wave troughs, and along the distance from the wave crest to the wave trough over one wavelength are investigated. The horizontal and vertical velocity components and the pressure in the fluid domain agree well with the analytical results.

Keywords: nonlinear water wave; smoothed particle hydrodynamics; velocity profile; pressure variation

1. Introduction

Wave load dominates the hydrodynamic effects on man-made structures in the ocean. The design of offshore structures requires detail information of loads and pressures exerted on the structures by ocean waves. Wave force can be investigated by physical test or numerical simulation. Physical tests are indispensable; however, they have some disadvantages which make physical modelling challenging. The cost of the model and the time for setting up are unavoidable. Moreover, the physical tests might face the impact of scaling problems for large structures. The analysis, design and optimisation of virtual models might be required before building a physical model for testing. This has led scientists to develop numerical tools.

Numerical wave simulation has been performed using a variety of methods. To solve the Navier-Stokes equations, the Lagrangian and the Eulerian are the two approaches. The Eulerian approach has been applied to study waves for decades. Nevertheless, the Eulerian method still faces the

∗Corresponding author, Professor, E-mail: basub@tcd.ie
[a] Ph.D., E-mail: nguyen.dinh@ucc.ie
[b] Ph.D. Student, E-mail: nguyenho@tcd.ie

http://www.techno-press.org/?journal=ose&subpage=7 ISSN: 2093-6702 (Print), 2093-677X (Online)

challenge of simulating large deformations and violent surface interactions which require special meshing techniques on the surface boundary. On the other hand, the Lagrangian approach is naturally suited for large deformation problems (Monaghan 1994) since it requires no special treatment for monitoring and recreating free surface. Because of these, the Smoothed Particle Hydrodynamics (SPH) which is a Lagrangian method has received attention from scientists and engineers.

In the literature, there has been many studies on simulation of wave using SPH (Liu and Liu 2010, Gotoh *et al.* 2018, Aly *et al.* 2011). Khayyer *et al.* (2008) proposed Corrected Incompressible Smoothed Particle Hydrodynamics method (CISPH) to monitor surface profile in breaking waves. Altomare *et al.* (2014) presented the study on numerical simulation of the complex geometries of breakwaters. Since the main objectives of the paper were the run-up values and breakwaters geometries, the surface wave elevation was monitored at a position which is closest to the wave paddle. Didier *et al.* (2014) studied the interaction of an incident regular wave and a vertical wall of a breakwater. The numerical wave height was validated with the experimental results however the numerical free surface elevation shows that the numerical model slightly underestimated the free surface elevation. Only the pressure on the wall was monitored while the variation of the pressure within the fluid domain was neglected. Altomare *et al.* (2015, 2017) reported a comprehensive study of wave generation and wave absorption using Weakly Compressible Smoothed Particle Hydrodynamics (WCSPH). The authors introduced applicability of SPH on examining wave loads on structures. The regular and irregular wave profiles were examined. The water surface was the main character for assessing the success of the numerical simulations (Altomare *et al.* 2015). In Altomare *et al.* (2017), the authors recommended the parameters for the SPH model using the DualSPHysics code. The SPH models of regular and irregular waves in a numerical wave tank were described in detail, the wave properties, such as water surface elevation and velocity fields, are shown. Omidvar *et al.* (2015) identified the disadvantage of artificial viscosity that aspects water surface representation. Chang *et al.* (2017) proposed a new SPH method where generated wave properties agreed well with the Second order Stokes' wave. Recently, Verbrugghe *et al.* (2018) coupled Finite Volume Method and the DualSPHysics code to simulate nonlinear wave in a large domain. In the above studies, the properties of the modeled wave, which are the surface amplitude, pressure, and velocity field, are studied and validated with the results from analytical methods and experimental simulations. However, the distributions and profiles of pressure and velocity field beneath the surface within the fluid domain are not completely examined. The previous studies mostly focused on the pressure and velocity at a specific position under generated wave. Hence, the objective of this paper is to investigate pressure and velocity variations within the fluid domain.

Properties of the generated wave by linear theory have been mathematically described in many studies. The wave properties such as velocity field, pressure distribution and particle kinematics under a progressive wave were studied in (Lamb 1993, Milne-Thomson 1996, Dean and Dalrymple 1991). Constantin and colleagues developed the study of Stokes' wave by mathematically investigating the nonlinear Euler equations for fluid flow properties in a fluid domain (Constantin and Strauss 2004, Constantin 2006, Constantin and Strauss 2010, Constantin 2013, 2016). Okamoto and Shōji (2016) used another approach to prove Constantin's finding and confirmed Constantin's conclusion on particle trajectory. Basu (2016, 2017) applied the nonlinear wave model to study the interaction of the surface wave and the underlying current and developed an estimation of the wave height based on pressure data on the seabed. Since the aim of the present study is to analyse the flow properties under a progressive water wave, the numerical simulation results are validated against the exact results from nonlinear wave theory (Constantin and Strauss 2004).

To investigate the behaviour of flow beneath the numerically generated wave, a steady wave propagating over still water in a two-dimensional wave flume is numerically modeled. DualSPHysics which is an SPH code has been used in this research to generate the nonlinear waves. The DualSPHysics code was first introduced by Crespo *et al.* (2011) and the latest version DualSPHysics_v5.0.3 released in 2020 includes the basic examples of SPHysics and added new features. This code has been used in wave simulation (Altomare *et al.* 2015, 2017, 2014) and the simulated results have shown a good agreement with experimental tests. We first simulate a numerical wave train using DualSPHysics and then study the flow properties within the fluid domain over one wavelength. The velocity and pressure fields are investigated and the variation of these are validated against recently obtained exact qualitative results from the full nonlinear Euler equations (Constantin 2016).

The rest of the paper is organized as follows. The SPH method and the exact qualitative results from the non-linear water wave theory are summarized in Section 2. Then, the numerical simulation is described in detail in Section 3. Numerical flow velocities and pressure distributions are studied and validated against the exact qualitative results in Section 4.

2. Methodology

2.1 Nonlinear model of water waves and exact qualitative results

A two-dimensional periodic water wave in the (x, y) plane, propagating over a still water region, has a velocity field $(u(x, y), v(x, y))$. The wave is formed by the balance between gravity and inertia force, without considering Coriolis effect, capillary, and viscous force. The still water depth is d and free surface is denoted by $y = \eta(x)$. The flow is irrotational, inviscid, and incompressible. The bottom boundary is impermeable and flat. The pressure at the free surface is constant and equals to the atmospheric pressure $P = P_{atm}$. A solution of period L to the governing equations for periodic traveling Stokes waves is provided by Constantin and Strauss (2004). The wave propagates over the still water region.

The fundamental equations of motion of the waves in a moving frame $(x - ct)$ given by the Euler equations are

$$\begin{cases} (u-c)u_x + vu_y = -P_x \ \text{ in } -d < y < \eta(x-ct), \\ (u-c)v_x + vv_y = -P_y - g \ \text{ in } -d < y < \eta(x-ct), \\ u_x + v_y = 0 \ \text{ in } -d < y < \eta(x-ct), \\ u_y = v_x \ \text{ in } -d < y < \eta(x-ct), \\ v = (u-c)\eta_x \ \text{ on } y = \eta(x-ct), \\ P = P_{atm} \ \text{ on } y = \eta(x-ct), \\ v = 0 \ \text{ on } y = -d, \end{cases} \tag{1}$$

where, c is the wave speed and t is the time variable. Using a stream function formulation, we get the system of equations

$$\begin{cases} \Delta\psi = 0 \ \text{ in} - d < y < \ \eta(x), \\ \frac{|\nabla\psi|^2}{2} + g(y+d) = Q \ \text{ on } \ y = \ \eta(x), \\ \psi = 0 \ \text{ on } \ y = \ \eta(x), \\ \psi = m \ \text{ on } \ y = \ -d, \end{cases} \tag{2}$$

where, m is a scalar constant called the mass flux.

The stream functions are constant along the upper and the bottom boundaries and can be written as

$$\psi(x,y) = m + \ \int_{-d}^{y}[u(x,s) - c]ds. \tag{3}$$

Due to Eq. (3), the streamlines $\psi = k$ with $k \in [0,m]$ provide a foliation of the closure $\bar{\Omega}$ of the fluid domain Ω, where the free surface corresponds to $\psi = 0$ and the flatbed to $\psi = m$. The wavelength is normalised with $L = 2\pi$, and it is assumed that in the moving frame the wave crest is at the point $(0,\eta(0))$ and the wave troughs are at the points $(\pm\pi,\eta(\pm\pi))$. Denote

$$\begin{cases} \Omega_+ = (x,y) \in \boldsymbol{\mathcal{R}}^2 : x \in (0,\pi), -d < y < \ \eta(x), \\ \Omega_- = (x,y) \in \boldsymbol{\mathcal{R}}^2 : x \in (-\pi,0), -d < y < \ \eta(x), \end{cases} \tag{4}$$

and let

$$S_+ = x \ \in (0,\pi), y = \ \eta(x); \ S_- = x \ \in (-\pi,0), y = \ \eta(x)$$

be the two halves of the free surface S in one period of the fluid domain Ω, and further

$$B_+ = x \ \in (0,\pi), y = \ d; \ B_- = x \ \in (-\pi,0), y = \ -d$$

be the two halves of the flatbed B. The crest line is $x = 0, d < y < \eta(0)$ while the trough line is $x = \pm\pi, d < y < \eta(\pm\pi)$. By assumption, the wave profile is symmetric about the crest and $\eta_x \leq 0$ on S_+. Further details are available in (Constantin 2011). The exact results are summarized as follows.

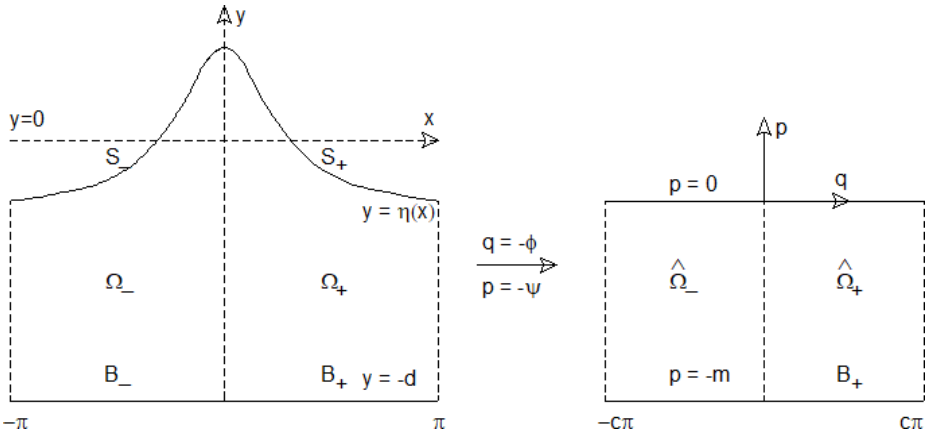

Fig. 1 Transformation of the domain

The horizontal velocity component u decreases along the three sides of the domain, Ω_+, from the wave crest to the wave trough. The resulting inequalities are

$$\begin{cases} u_y(0,y) > 0 \text{ for } y \in \big(d,\eta(0)\big), \\ u_x(x,d) < 0 \text{ for } x \in (0,\pi), \\ u_y(\pi,y) < 0 \text{ for } y \in (d,\eta(\pi)). \end{cases} \tag{5}$$

In addition, the vertical component of the velocity is proved to be equal to 0 along three sides of the flow domain from the wave crest to the wave trough

$$\begin{cases} v_y(0,y) = 0 \text{ for } y \in \big(d,\eta(0)\big), \\ v_x(x,-d) = 0 \text{ for } x \in (0,\pi), \\ v_y(\pi,y) = 0 \text{ for } y \in (d,\eta(\pi)). \end{cases} \tag{6}$$

Considering the pressure variation, Constantin and Strauss (2004) stated that the minimum pressure is equal to 0 along the free surface, while the maximum is at the point on the flatbed directly under the wave crest.

2.2 Smoothed particle hydrodynamics

Smoothed Particles Hydrodynamics (SPH) is a Lagrangian method for computational fluid dynamics which considers flow comprising of particles. In SPH, each particle has its own density and velocity, thus the change of the properties of the flow field is also associated with the change in particle properties. At each time step, the particle properties are updated by interpolating properties of the neighboring particles. The driving external force in this case is gravity only.

Any continuous quantities of fields, their gradients and Laplacian can be approximated using SPH formulas. The fundamental Navier-Stokes equations for flow are expressed in an SPH form for a particle with index $'a'$, as follows

$$\frac{d\ \boldsymbol{v}_a}{dt} = -\sum_b m_b \left(\frac{p_a}{\rho_a^2} + \frac{p_b}{\rho_b^2} + \Pi_{ab}\right) \nabla_a W_{ab} + \boldsymbol{g} \tag{7}$$

$$\frac{d\ \rho_a}{dt} = \sum_b m_b (\boldsymbol{v}_a - \boldsymbol{v}_b) \nabla_a W_{ab} \tag{8}$$

where, m, ρ, p and $\boldsymbol{v}$ are the mass, density, pressure, and velocity respectively with the subscript denoting index for the individual particles. In addition, in Eqs. (7) and (8), $\boldsymbol{g}$ is the gravitational acceleration, W_{ab} is the kernel function and $\nabla_a W_{ab}$ is the gradient operator taken with respect to particle $'a'$ in a discrete form defined between particles with index $'a'$ and $'b'$.

The viscous force term Π_{ab} between two particles with indices $'a'$ and $'b'$ has a general form

$$\Pi_{ab} = \begin{cases} \frac{-\alpha \bar{c}_{ab} \mu_{ab} + \beta \mu_{ab}^2}{\bar{\rho}_{ab}}; & \boldsymbol{v}_{ab}.\boldsymbol{r}_{ab} < 0; \\ 0; & \boldsymbol{v}_{ab}.\boldsymbol{r}_{ab} > 0. \end{cases} \tag{9}$$

The value of $\alpha = 0.01$ and $\beta = 0$ have been proven to give the best results by validation from wave flumes studies on wave propagation and wave loading exerted onto structures (Altomare *et al.* 2015). The terms $\boldsymbol{r}_{ab} = \boldsymbol{r}_a - \boldsymbol{r}_b$ and $\boldsymbol{v}_{ab} = \boldsymbol{v}_a - \boldsymbol{v}_b$ correspond to the relative position and velocity respectively between particles with indices $'a'$ and $'b'$. The term $\bar{c}_{ab} = 0.5(c_a + c_b)$ is

the mean speed of sound, $h = 0.5(h_a + h_b)$ is the mean smoothing length, $\bar{\rho}_{ab} = 0.5(\rho_a + \rho_b)$ is the mean density and $\mu_{ab} = h\boldsymbol{v}_{ab}.\boldsymbol{r}_{ab}/(\boldsymbol{r}_{ab}^2 + \eta^2)$ is calculated with $\eta^2 = 0.01h^2$.

The rate of change of particle position $\boldsymbol{r}_a$ for a particle with index $'a'$ is

$$\frac{d\boldsymbol{r}_a}{dt} = \boldsymbol{v}_a. \tag{10}$$

The kernel function is a function of the ratio $q = r/h$, where $r = |\boldsymbol{r}_{ab}|$ is the distance between particle $'a'$ and particle$'b'$, while h is the smoothing length, specifying the controlled area around particle $'a'$ in which the number of neighboring particles are calculated. In this study, Quintic kernel function is chosen

$$W(r,h) = \alpha_D \left(1 - \frac{q}{2}\right)^4 (2q+1); 0 \leq q \leq 2 \tag{11}$$

with α_D equals to $7/4\pi h^2$ in two-dimensional simulations.

For compressible fluid, the speed of sound is much greater than the bulk velocity of the sound in the flow. To model the incompressible flow in SPH, the equation of state is modified to give a smaller speed of sound which is typically a factor of 10 greater than the speed of the bulk motion. The accurate equation of state (Batchelor 2000) was modified to give a smaller speed of sound used in the pressure equation

$$p_a = B\left(\left(\frac{\rho_a}{\rho_0}\right)^\gamma - 1\right) \tag{12}$$

in which $\gamma = 7$ in case of water; p_a is the pressure of particle $'a'$; ρ_0 is the reference density, which is approximately 1000 kg/m^3; ρ_a is the particle density from the continuity equation; $B = c_0^2\rho_0/\gamma$ is the maximum limit of the density with c_0 as the speed of sound at the reference density. The choice of c_0 ensures the weakly-compressible regime in which the density fluctuation is within 1%. The density variation in fluid flow is approximately M^2, where M is the Mach number (Monaghan (1994)). If $\Delta\rho \approx 0.01\ \rho_0$, $M = max_t(||\vec{u}||)/\ c_0 < 0.1$,where $max_t(||\vec{u}||)$ is the maximum intensity of the velocity expected in the flow time evolution. Hence, the first constraint for the speed of sound is $c_0 \geq 10max_t(||\vec{u}||)$. For gravity wave simulation, the wave celerity might be larger than the fluid flow velocity, thus other constraint of the speed of sound results from the wave celerity, $c_w^2 = gtanh(kH)/k$ where d is the still water depth, k is the wave number. When $kd \rightarrow 0$, the wave celerity becomes $c_w^2 = \sqrt{gd}$. Choosing $c_0 = 10\sqrt{gd}$ leads to the condition of the speed of sound $c_0 \geq 10\max\left(\sqrt{gd}, max_t\left(||\vec{u}||\right)\right)$ (Antuono *et al.* 2011, Marrone 2012). To provide uniform particle distribution and a regular pressure field, δ-Plus-SPH scheme is derived (Sun *et al.* 2019) using quasi-Lagrangian approach. In this study, this approach is not applied since the main purpose is the variation of the pressure in the flow field rather than the stability of the particle pressure.

2.2.1 Time stepping algorithm

Symplectic time integration algorithm is applied in this work. The corrected velocity is calculated from the position and the density at the middle of the time step as follows

$$\begin{aligned} \boldsymbol{r}_a^{n+\frac{1}{2}} &= \boldsymbol{r}_a^n + \frac{\Delta t d\boldsymbol{r}_a^n}{2\ dt}, \\ \rho_a^{n+\frac{1}{2}} &= \rho_a^n + \frac{\Delta t d\rho_a^n}{2\ dt}, \end{aligned} \tag{13}$$

where the pressure $p_a^{n+\frac{1}{2}}$ is calculated using the equation of state in Eq. (12). The superscript n denotes the time step index and the time step is Δt. Then, the field properties are calculated at the next time step according to

$$\begin{aligned} \boldsymbol{v}_a^{n+1} &= \boldsymbol{v}_a^n + \Delta t \frac{d\boldsymbol{v}_a^{n+\frac{1}{2}}}{dt}, \\ \boldsymbol{r}_a^{n+1} &= \boldsymbol{r}_a^n + \frac{\Delta t}{2}\left(\frac{d\boldsymbol{r}_a^n}{dt} + \frac{d\boldsymbol{r}_a^{n+\frac{1}{2}}}{dt}\right), \end{aligned} \tag{14}$$

and the updated value of density $d\rho_a^{n+1}/dt$ is calculated by the value of $\boldsymbol{v}_a^{n+1}$ and $\boldsymbol{r}_a^{n+1}$.

2.2.2 Boundary condition

We use Dynamic Boundary Condition (DBC) which is available in DualSPHysics code (Crespo *et al.* (2015)). The boundary particles satisfy the fundamental equations; however, they are forced to remain at the fixed positions. Thus, the boundary particles can automatically generate a repulsive force on their neighboring fluid particles resulting from the change of their density when the fluid particles approach them.

2.2.3 Wave generation and wave absorption

We implement the second order Stokes wave model based on (Madsen 1971) which is an inbuilt function in DualSPHysics code. The wave is generated by a numerical piston type wave-maker whose displacement is equal to

$$e(t) = \frac{S_0}{2}\sin(\omega t + \delta) + \left[\left(\frac{H^2}{32\ d}\right)\left(\frac{3\ \cosh(kd)}{sinh^3(kd)}\right) - \frac{2}{m_1}\right]\sin(2\omega t + 2\delta) \tag{15}$$

in which

$$m_1 = \frac{2\ sinh^2(kd)}{\sinh(kd)\cosh(kd)+kd}. \tag{16}$$

The piston stroke is $S_0 = H/m_1$ and δ is an unknown phase angle. This equation is applicable for the waves that comply with the condition given by $HL^3/d^3 < 8\pi^2/3$ in which H is the wave height, d is the still water depth, $k = 2\pi/L$ is the wave number and ω is the angular frequency.

In order to avoid the wave reflection and to prolong the simulation, the right boundary of the domain has a passive beach absorption. The dissipating beach is straightforward and easy to apply and Altomare *et al.* (2017) shows that the beach has good dissipation result compared with the passive wave absorption. In this work, we use a dissipating beach because of its simplicity.

3. Numerical simulation

3.1 Computational domain

Fig. 2 shows dimensions of the wave flume. A wave paddle on the left-hand side creates a nonlinear wave, its height (h_w) is 2 m. The flatbed length is $L1 = 11$ m. The beach on the

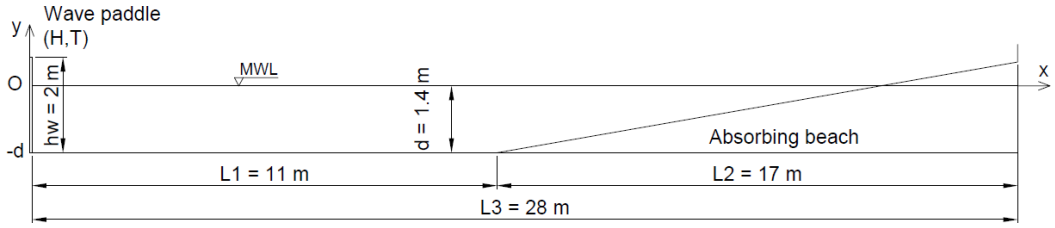

Fig. 2 Sketch of numerical wave flume

right-hand side is $L2 = 17$ m long and the total length of the wave flume is $L3 = 28$ m. The beach on the right-hand side acts as a passive wave absorption. Its slope is 1:10. The water depth d is 1.4 m, comparing with the wave height ($H = 0.2$ m) and the wave period ($T = 1.31$ s), the wave falls into the deep-water wave category. This assumption fits the conclusion of Constantin (2011) in which the Stokes wave is suitable for modelling deep water small amplitudes waves. A viscous damping zone (Zhang *et al.* 2017) is not considered in the present case since it was not implemented at the numerical model at this stage. Moreover, the main purpose of this study focuses on the flow properties; hence the choice of absorbing beach is for simplicity.

The resolution of the model (i.e., the inter-particle distance) decides the total simulation time and it affects the wave height interpolation in following part of the research. In case of wave generation simulation, Altomare *et al.* (2017) studied five different resolutions and the authors have suggested that the ratio of the wave height to the distance between particles (dp) should be higher than 10. It is not necessary that a finer resolution will substantially improve the model accuracy. In the next section, simulation results with three different inter-particle distance $dp = 0.005$ m, $dp = 0.01$ m, and $dp = 0.02$ m are examined. Based on these studies, we choose the initial distance among particles and the CFL coefficient for this research.

The simulation has been performed using DualSPHysics code on GPU-CPU, NVIDIA GPU card Quadro M4000. The computational capacity is 5.2, 13 cores, 8GB memory.

4. Results and discussions

To study the flow properties, it is first necessary to examine whether the waves can be successfully generated and to determine the positions of the wave crest and the wave trough in the numerical wave tank.

4.1 Wave generation

Fig. 3 shows the wave generated at $t = 16.78$ s. The phenomenon of wave height decaying along the length of the flume is discussed in (Lind *et al.* 2012, Altomare *et al.* 2017, Omidvar *et al.* 2015, Chang *et al.* 2017). The instability of the pressure field, the boundary condition and the kernel function properties considered are the main reasons for this wave height decay. Despite this discrepancy, we use such a wave in this paper over the region where the wave height is almost constant. We aim to study the flow properties under surface waves; thus, we investigate these properties under the wave crest and the wave trough within one wavelength. There are three crests and three troughs on the region with flatbed which are presented in Table 1. The flow properties will be discussed further in the following sections.

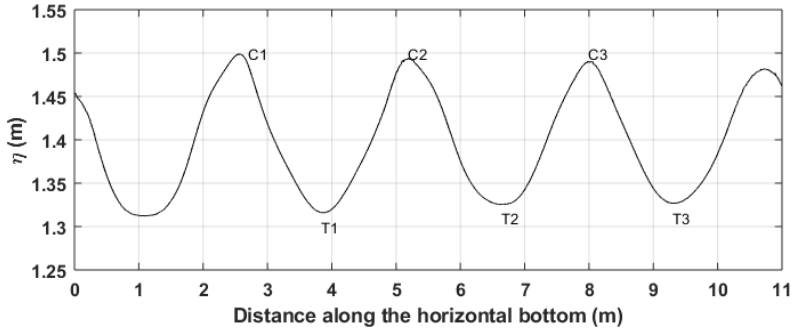

Fig. 3 The surface elevation for regular wave at $t = 16.78$ s

Table 1 Wave crest and wave trough positions

Crest	x-position (m)	Trough	x-direction (m)
C1	2.56	T1	3.84
C2	5.18	T2	6.64
C3	7.98	T3	9.30

4.2 Convergence study

The purpose of this section is to examine the effect of distance between particles on flow properties including velocity and pressure field. The simulations are set up with different initial distances among the particles and a constant CFL number to examine the effect of the initial distances. Three different resolutions $dp = 0.005$ m, $dp = 0.01$ m, and $dp = 0.02$ m are considered. The first simulation (with $dp = 0.005$ m) takes 25 hours to complete while the second and the third one with $dp = 0.01$ m and $dp = 0.02$ m takes 3.9 hours and 36 minutes, respectively.

The horizontal and vertical velocity profiles under the three crests are shown in Fig. 4 to Fig. 6. In Fig. 4, the horizontal velocity under the wave crest C1 for the three wave simulations are quite similar, however, the profiles of vertical velocity under the crest exhibit some differences from each other. At locations near the free surface, the horizontal velocity decreases from 0.4 m/s at C1 to 0.3 m/s at C3. Horizontal velocity also reduces as we move away from the wave paddle. However, this is possibly related to similar reason accounting for the spurious decrease in wave height as discussed in Section 4.1. Regarding the vertical component of the velocity under the three crests, which fluctuate around 0 m/s over the depth of the water, no significant differences have been observed.

Next, we study the variation of horizontal and vertical velocity components along the bottom boundary from the point under the first wave crest to the first wave trough. The horizontal and vertical velocities are plotted in Fig. 7. There are different trends observed in both cases. The vertical velocity varies slightly around 0 m/s, as shown in Fig. 7a. With $dp = 0.005$ m simulation shows a large fluctuation at positions close to the point under the wave trough. Fig. 7b reveals a significant fluctuation in horizontal velocity field. The fluctuations are due to numerical effects near the boundary as discussed previously. Even though there are fluctuations in the horizontal velocity field observed in Fig. 7b for the simulation with $dp = 0.005$ m, a decreasing trend in the amplitude

of the horizontal velocity is seen. The other two simulations (with $dp = 0.01$ m and $dp = 0.02$ m) are unable to capture this trend. The horizontal velocity at the flatbed has been proved to be monotonically decreasing from the point under a wave crest to the point under a wave trough Constantin (2013), however Fig. 7(b) is unable to represent the analytical conclusion clearly. These results further support the idea of unstable velocity field near the boundaries for SPH.

Fig. 8 shows the variation of total pressure under the first wave, along the crestline and the trough line. Simulations with $dp = 0.005$ m and $dp = 0.01$ m describe a similar pressure profile. It is observed from Fig. 8 that for the simulation with $dp = 0.02$ m, the pressure rises sharply near the flatbed. The sharp increase in pressure seen in Fig. 8 might be due to the boundary effects in SPH simulation.

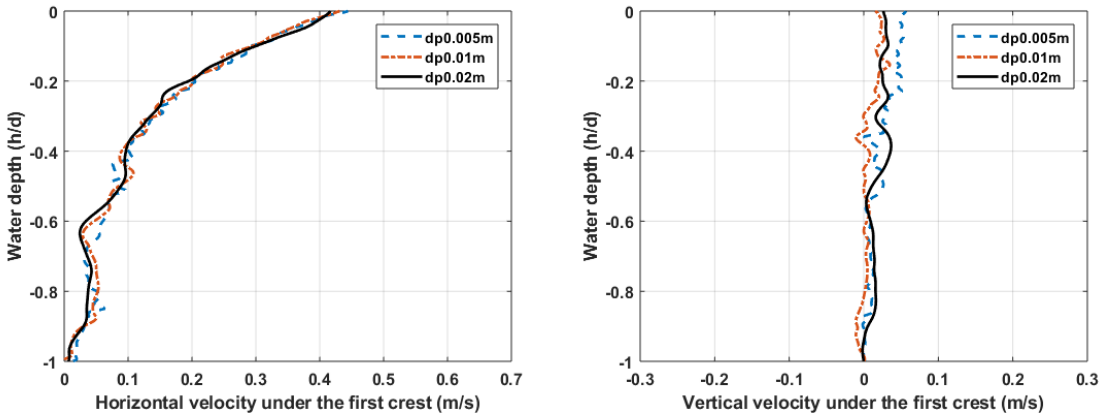

(a) (b)

Fig. 4 Velocity with three different initial distance among particles $dp = 0.005$ m, $dp = 0.01$ m, and $dp = 0.02$ m under C1

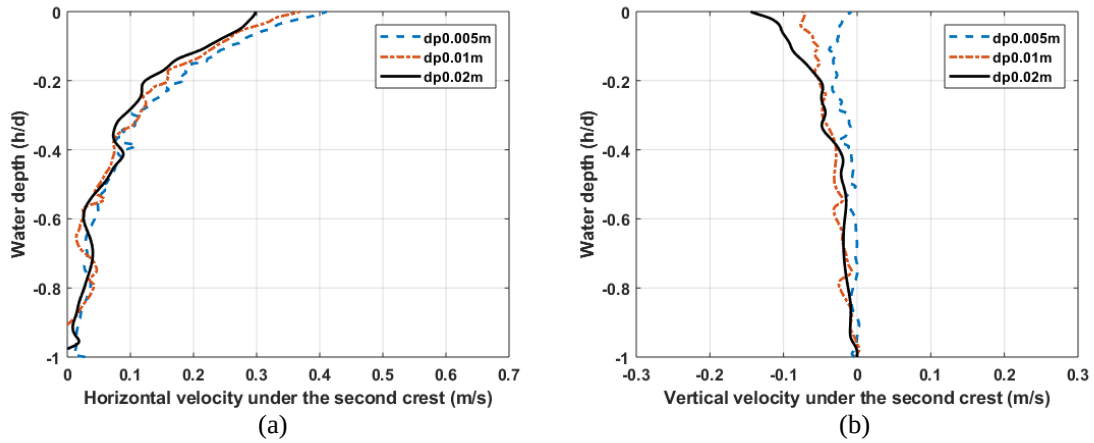

(a) (b)

Fig. 5 Velocity with three different initial distance among particles $dp = 0.005$ m, $dp = 0.01$ m, and $dp = 0.02$ m under C2

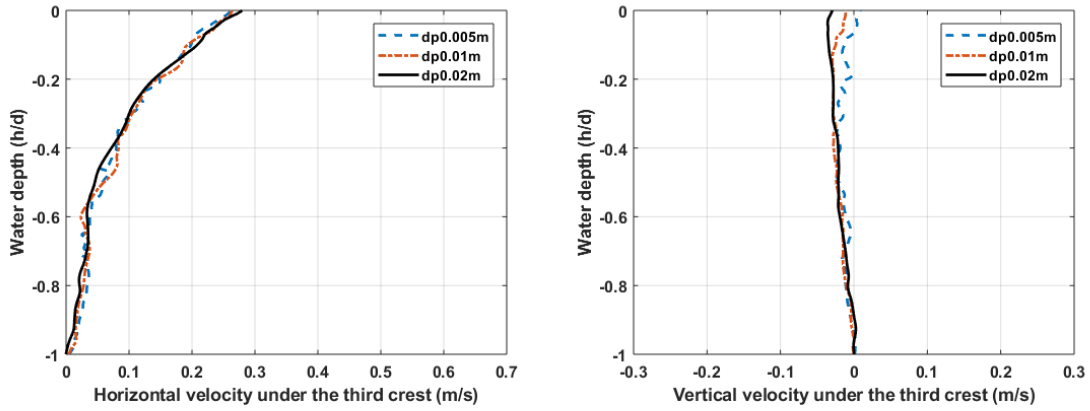

(a) (b)

Fig. 6 Velocity with three different initial distance among particles $dp = 0.005$ m, $dp = 0.01$ m, and $dp = 0.02$ m under C3

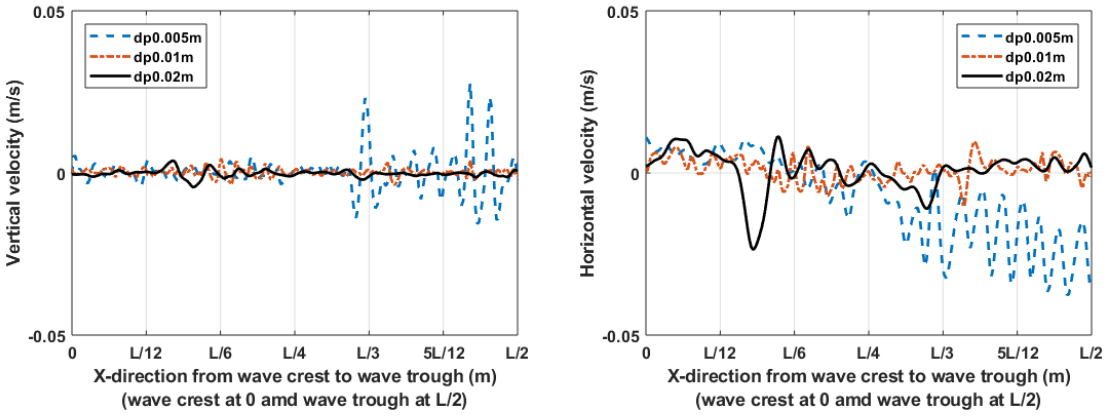

(a) (b)

Fig. 7 Velocity variation in horizontal direction at seabed elevation with three different initial distance among particles $dp = 0.005$ m, $dp = 0.01$ m, and $dp = 0.02$ m

Taken together, these results suggest that the initial conditions for this study are sufficient. The next section, therefore, moves on to discuss the variation of flow properties under the generated surface waves in terms of velocity and pressure field over one wavelength and compare with the existing exact results.

In this study, the wave height is 0.2 m and the chosen distance between particles is 0.005 m, thus the ratio (H/dp) is 40. The CFL number of 0.1 has been chosen for stability reason. Moreover, the ratio of the still water level to the distance between particles (d/dp) is 280 ensuring no inaccuracies in the initial setup.

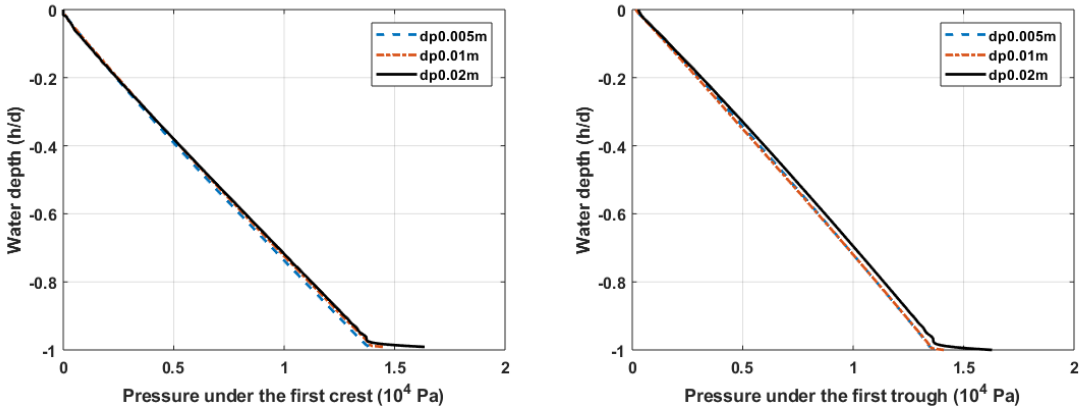

(a) (b)

Fig. 8 Pressure with three different initial distance among particles $dp = 0.005$ m, $dp = 0.01$ m, and $dp = 0.02$ m

4.3 Variation of horizontal velocity

Fig. 9(a) shows the horizontal velocity under the wave crests while Fig. 9(b) describes those under the wave trough. The velocity distributions agree with previous studies of (Lind *et al.* 2012); the maximum values of horizontal velocity are located at the free surface and the minimum ones are at the bottom. The horizontal velocity along the depth in Fig. 9(a) follows Eq. (5) in which the horizontal velocity decrease with the depth. On the other hand, the horizontal velocity under the wave trough is negative and decreases from the flatbed to the surface.

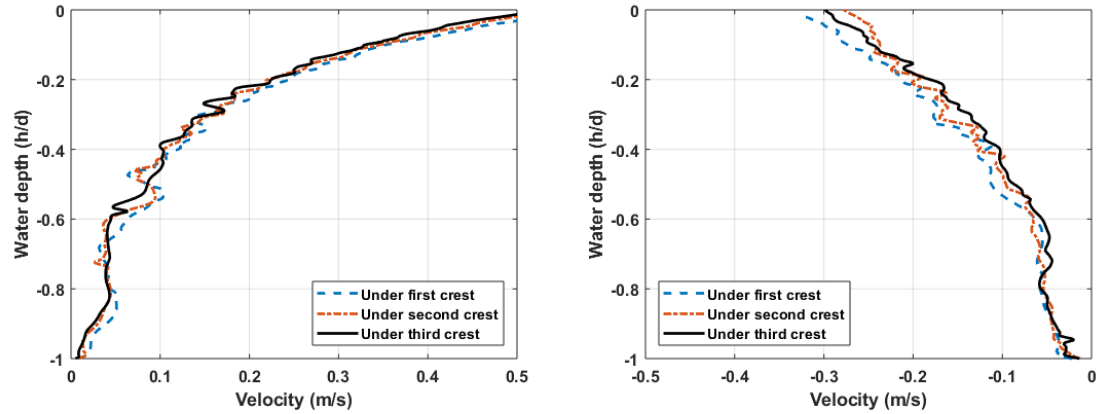

(a) Horizontal velocity under crest (b) Horizontal velocity under trough

Fig. 9 Comparison of horizontal velocity profile as a function of the normalized water depth h/d

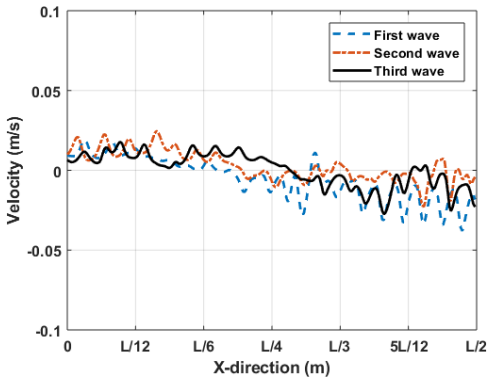

Fig. 10 Comparison of the velocity profile at the bottom from the wave crest to the wave trough

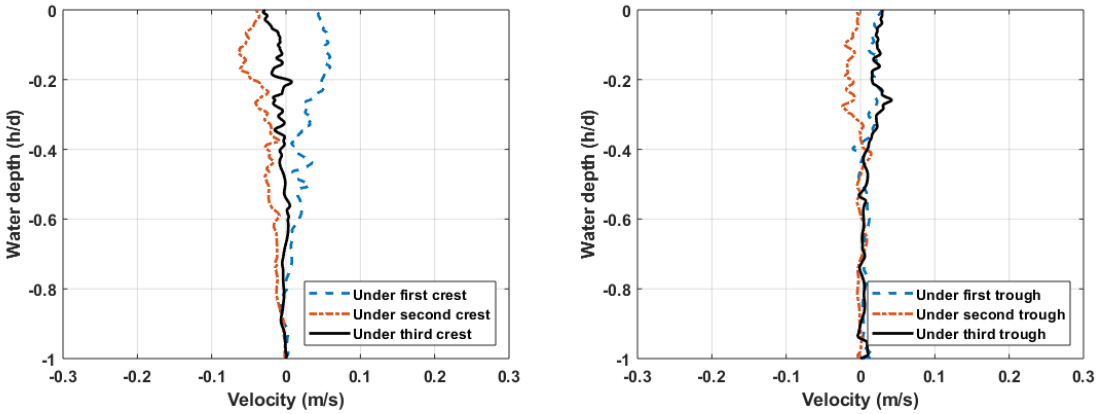

(a) Vertical velocity under crest (b) Vertical velocity under trough

Fig. 11 Comparison of vertical velocity profile as a function of the normalized water depth h/d.

The variation of the horizontal velocity in the propagating direction of the wave is shown in Fig. 10. The crest line is at 0 and the trough line is at $L/2$, where L is the length of the wave. It is clearly seen from Fig. 10 that the velocity changes sign at a unique point (Constantin 2006), thus the velocity from $L/4$ to $L/2$ is smaller than 0. Then, a decreasing trend from the point under the crest to the point under the trough is seen which has been predicted from theoretical results (Eq. (5)). In addition, a considerable variation of the velocity is observed in the vicinity of the point directly under the trough. One possible cause of this is the effect of boundary condition which is mentioned in (Chang *et al.* 2017, Omidvar *et al.* 2012).

4.4 Variation of vertical velocity

The vertical velocity profiles are plotted in Figs. 11(a) and 11(b). Fig. 11(a) shows the variation of the velocity under the wave crest. The vertical component fluctuates more near the free surface.

The fluctuation is stronger at the crest line (Fig. 11(a)) than at the trough line (Fig. 11(b)). Moreover, the velocity under the third crest is more stable than the first two crest, hence the variation of the vertical velocity might depend on the distance from the wave paddle. This phenomenon is not so clearly seen for the case under the wave trough. The vertical velocities under the wave trough have the same pattern and they fluctuate more in the vicinity of the free surface than in deeper regions.

Along the propagating direction of the wave, the vertical velocity on the flatbed is more stable than the horizontal components, as shown in Fig. 12. Fig. 12 shows the variation of the vertical velocity along x-direction in the range of -0.02 m/s to 0.02 m/s. Fluctuations are greater for the point on the bed near the wave trough than near the wave crest. This may result from the compression of the particles under the wave trough leading to an unstable pressure region, hence unstable pressure field affects the velocity of the particles. Note that for the simulation considered the vertical velocity on the flatbed should be identically zero (as expected from the exact results).

4.5 Variation of pressure

The pressure distribution under three crests and troughs are shown in Figs. 13 and 14, respectively. The pressure strictly decreases from the bottom depth to the free surface. It is difficult to conclude that the maximum pressure is at the point directly under the wave crest (as expected from the exact results in Section 2.1) based on Fig. 13 only, however the pressure shows a downward trend along the flatbed (though numerical fluctuations are unavoidable) from the wave crest to the wave trough in Fig. 14. Hence, the points of maximum pressure are located at the bottom depth and under the crests. These findings confirm the qualitative success of the numerical simulation comparing with the exact results from the nonlinear water wave model governed by the full nonlinear Euler equations.

A good agreement was globally observed between numerical results and analytical results in Eqs. (5) and (6). The velocity profile distributions along the depth of the water obtained with the numerical model were globally similar to the analytical inequalities. The similar trends were observed throughout the pressure field.

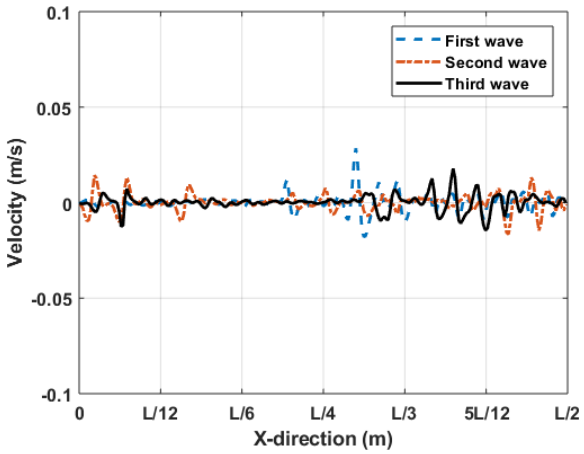

Fig. 12 Comparison of the velocity profile at the bottom from the wave crest to the wave trough

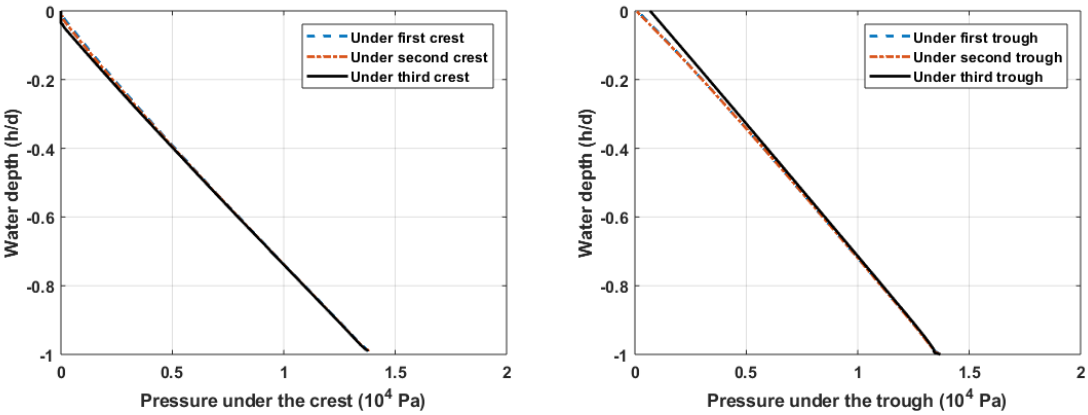

Fig. 13 Comparison of pressure profile as a function of the normalized water depth h/d.

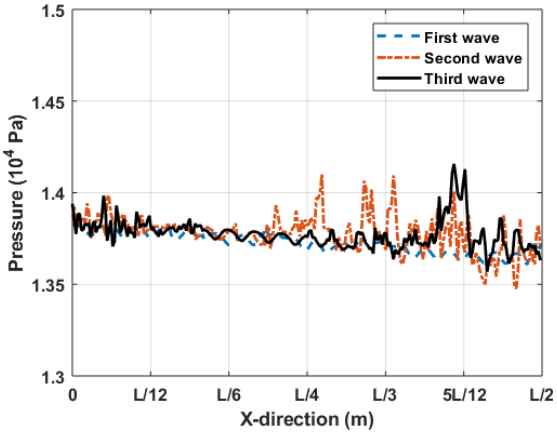

Fig. 14 Comparison of the pressure profile at the bottom from the wave crest to the wave trough

5. Conclusions

An SPH model is used to simulate the regular wave train in a numerical wave flume. To achieve this verification, the velocity profiles under wave crests and wave troughs are examined. Similarly, the pressure along straight lines under wave crests and wave troughs are studied. The numerical simulation results match the trend closely with the exact qualitative results available from the nonlinear water wave theory confirming the success of the simulation carried out.

Some fluctuations in velocity and pressure profiles near the boundary close to the bed and at the surface have been observed which will require some attention and improvement in the numerical model.

References

Altomare, C., Crespo, A.J., Domínguez, J.M., Gómez-Gesteira, M., Suzuki, T. and Verwaest, T. (2015), "Applicability of Smoothed Particle Hydrodynamics for estimation of sea wave impact on coastal structures", *Coast. Eng.*, **96**, 1-12.

Altomare, C., Crespo, A.J., Rogers, B., Domínguez, J.M., Gironella X. and Gómez-Gesteira, M. (2014), "Numerical modelling of armour block sea break-water with smoothed particle hydrodynamics", *Comput. Struct.*, **130**, 34-45.

Altomare, C., Domínguez, J.M., Crespo, A.J., González-Cao, J., Suzuki, T., Gómez-Gesteira, M. and Troch, P. (2017), "Long-crested wave generation and absorption for SPH-based Dualsphysics model", *Coast. Eng.*, **127**, 37-54.

Aly, A.M., Asai, M. and Sonoda, Y. (2011), "Simulation of free falling rigid body into water by a stabilized incompressible SPH method", *Ocean Syst. Eng.*, **1**(3), 207-222.

Antuono, M., Colagrossi, A., Marrone, S. and Lugni, C. (2011), "Propagation of gravity waves through an SPH scheme with numerical diffusive terms", *Comput. Phys. Commun.*, **182**(4), 866-877.

Basu, B. (2016), "Irrotational two-dimensional free-surface steady water flows over a flat bed with underlying currents", *Nonlinear Analysis: Theory, Methods & Applications*, **147**, 110-124.

Basu, B. (2017), "Estimation of wave heights from pressure data at the bed in the presence of uniform underlying currents", *Nonlinear Anal.*, **156**, 82-89.

Batchelor, G.K. (2000), *An introduction to fluid dynamics*, Cambridge University Press.

Chang, J., Liu, S.X. and Li, J.X. (2017), "A study of the stability properties in simulation of wave propagation with SPH method", *China Ocean Eng.*, **31**(2), 173-182.

Constantin, A. (2006), "The trajectories of particles in stokes waves", *Inventiones mathematicae*, **166**(3), 523-535.

Constantin, A. (2011), "Nonlinear water waves with applications to wave-current interactions and tsunamis", *CBMS-NSF Conference Series in Applied Mathematics*, **81**, SIAM, Philadelphia.

Constantin, A. (2013), "Mean velocities in a stokes wave", *Archive for Rational Mechanics and Analysis*, 1-11.

Constantin, A. (2016), "Extrema of the dynamic pressure in an irrotational regular wave train", *Phys. Fluids*, **28**(11), 113604.

Constantin, A. and Strauss, W. (2004), "Exact steady periodic water waves with vorticity", *Commun. Pure Appl. Math.*, **57**(4), 481-527.

Constantin, A. and Strauss, W. (2010), "Pressure beneath a stokes wave", *Commun. Pure Appl. Math.*, **63**(4), 533-557.

Crespo, A.J., Domínguez, J.M., Barreiro, A., Gómez-Gesteira, M. and Rogers, B.D. (2011), "GPUs, a new tool of acceleration in CFD: efficiency and reliability on smoothed particle hydrodynamics methods", *PloS one*, **6**, e20685.

Crespo, A.J., Domínguez, J.M., Rogers, B.D., Longshaw, S., Canelas, R., Vacondio, R., Barreiro, A. and García-Feal, O. (2015), "Dualsphysics: Open-source parallel CFD solver based on smoothed particle hydrodynamics (SPH)", *Comput. Phys. Commun.*, **187**, 204-216.

Dean, R.G. and Dalrymple, R.A. (1991), *Water wave mechanics for engineers and scientists*, World Scientific Publishing Company.

Didier, E., Neves, D.R.C.B., Martins, R. and Neves, M.G. (2014), "Wave interaction with a vertical wall: SPH numerical and experimental modeling", *Ocean Eng.*, **88**, 330-341.

Gotoh, H. and Khayyer, A. (2018), "On the state-of-the-art of particle methods for coastal and ocean engineering", *Coast. Eng.*, **60** (1), 79-103.

Khayyer, A., Gotoh, H. and Shao, S.D. (2008), "Corrected incompressible SPH method for accurate water-surface tracking in breaking waves", *Coast. Eng.*, **55** (3), 236–250.

Lamb, H. (1993), *Hydrodynamics*, Cambridge University Press.

Lind, S., Xu, R., Stansby, P. and Rogers, B.D. (2012), "Incompressible smoothed particle hydrodynamics for free-surface flows: A generalised diffusion-based algorithm for stability and validations for impulsive flows and propagating waves", *J. Comput. Phys.*, **231**(4), 1499-1523.

Liu, M. and Liu, G. (2010), "Smoothed particle hydrodynamics (SPH): an overview and recent developments", *Archives of Computational Methods in Engineering*, **17**(1), 25-76.

Madsen, O.S. (1971), "On the generation of long waves", *J. Geophys. Res.*, **76**(36), 8672-8683.

Marrone, S. (2012), "Enhanced SPH modeling of free-surface flows with large deformations", Ph.D. dissertation, University of Rome La Sapienza, Rome, Italy.

Milne-Thomson, L.M. (1996), *Theoretical hydrodynamics*, Courier Corporation.

Monaghan, J.J. (1994), "Simulating free surface flows with SPH", *J. Comput. Phys.*, **110**(3), 399-406.

Okamoto, H. and Shōji, M. (2012), "Trajectories of fluid particles in a periodic water wave", *Philos. T. Roy. Soc. A: Math. Phys. Eng. Sci.*, **370**(1964), 1661-1676.

Omidvar, P., Norouzi, H. and Zarghami, A. (2015), "Smoothed Particle Hydrodynamics for water wave propagation in a channel", *Int. J. Modern Phys. C*, **26**(8), 1550085.

Omidvar, P., Stansby P.K. and Rogers, B.D. (2012), "Wave body interaction in 2D using smoothed particle hydrodynamics (SPH) with variable particle mass", *Int. J. Numer. Meth. Fl.*, **68** (6), 686-705.

Sun, P.N., Colagrossi, A., Marrone, S., Antuono, M. and Zhang, A.M. (2019), "A consistent approach to particle shifting in the δ-Plus-SPH model", *Comput. Method. Appl. M.*, **348**, 912-934.

Verbrugghe, T., Domínguez, J.M., Crespo A.J., Altomare, C., Stratigaki, V., Troch, P. and Kortenhaus, A. (2018), "Coupling methodology for smoothed particle hydrodynamics modelling of non-linear wave-structure interactions", *Coast. Eng.*, **138**, 184-198.

Zhang, A.M., Sun, P.N., Ming, F.R. and Colagrossi, A. (2017), "Smoothed particle hydrodynamics and its applications in fluid-structure interactions", *J. Hydrodynamics*, **29** (2), 187-216.

AK